Ion Mobility-Mass Spectrometry Applied to Cyclic Peptide Analysis: Conformational Preferences of Gramicidin S and Linear Analogs in the Gas Phase

Brandon T. Ruotolo, Colby C. Tate, and David H. Russell

Laboratory for Biological Mass Spectrometry, Department of Chemistry, Texas A&M University, College Station, Texas, USA

In this paper, we present an investigation of the gas-phase structural differences between cyclic and linear peptide ions by matrix-assisted laser desorption ionization-ion mobility-mass spectrometry. Specifically, data is shown for gramicidin S (cyclo-VOLFPVOLFP where phenylalanines are D rather than L-type amino acids and the O designates the non-standard amino acid ornithine) and five linear gramicidin S analogues. Results are interpreted as evidence for a β-sheet (or β-hairpin) conformational preference in both linear-protonated and sodiated-cyclic gramicidin S gas-phase peptides, and a preference for the protonated-cyclic peptide to adopt a collapsed, random coil-type conformation. A comparison with solution-phase circular dicrhoism measurements is performed, and structures similar to those observed in the gas phase appear to be favored in low-dielectric solvents such as 2,2,2-triflouroethanol. The utility of ion mobility-mass spectrometry (IM-MS) as a means of rapidly distinguishing between linear and cyclic peptide forms in also discussed. (J Am Soc Mass Spectrom 2004, 15, 870−878) © 2004 American Society for Mass Spectrometry

Antimicorobial peptides are a varied class of biological molecules that are important as lead-compounds in multiple drug-design efforts [1–3]. Although specifics in terms of biological function are not known in many cases, several target molecules (including membrane-bound and internal cellular components) have been identified as key players in antimicrobial peptide activity [4]. Antibiotic function in peptides is, in most cases, not limited to a single cell type; such peptides often exhibit interactions with both prokaryotic and eukaryotic cells [5]. In addition, peptide antibiotics display a wide range of conformational preferences including α-helical, extended, and cyclic β-sheet-type structures [6]. The interaction of this diverse class of peptides with a preferred biological target (i.e., a lipid molecule on a microbial membrane) is thought to cause a conformational change in some peptide antibiotics, the study of which is an active area of research in several laboratories [7].

The peptide gramicidin S, a cyclic antimicrobial peptide having the amino acid sequence cyclo(VOLFPVOLFP) (where O designates the non-standard amino acid ornathine and the phenylalanine residue is a D-rather than L-amino acid), prefers a β-sheet type structure in solution as determined by several methods, with two type II′ β-turns positioned at opposite ends of the cyclic structure [8]. The activity of gramicidin S is, in part, attributed to the amphipathic nature of its β-sheet structure, where the primary amine functional groups of the ornathine side chains are situated on the opposite face of the molecule relative to the hydrophobic side chains of valine and leucine [9]. Gramicidin S displays both hemolytic and antimicrobial activity, for both gram− and gram+ bacteria, making the peptide unsuitable for use as a general antibiotic, and is generally restricted to topical applications [5]. Hodges and coworkers used gramicidin S as a model to develop a group of larger (14 amino acids in length) cyclic peptides that display potent antimicrobial activity for both gram+ and gram− bacteria and negligible hemolytic activity [4, 9]. Due to its relatively small size and lower degrees of freedom relative to linear peptides, gramicidin S is an excellent model for β-sheet formation in proteins. Recent studies, aimed at determining the influence of side chain identity on the stability of the type II′ β-turns found in native gramicidin S, suggest several factors influence the overall conformational stability of the peptide. For example, heterochirality of the backbone at the $i + 1$ and $i + 2$ positions relative to the β-turn, side chain N-alkylation, and proline-phenyalanine interactions all provide contributions to the overall stability of the β-sheet structure in cyclic gramicidin S analogues [10].

Published online April 9, 2004

Address reprint requests to Dr. D. H. Russell, Laboratory for Biological Mass Spectrometry, Department of Chemistry, Texas A&M University, College Station, TX 77843, USA. E-mail: russell@mail.chem.tamu.edu

1044-0305/04/$30.00
doi:10.1016/j.jasms.2004.02.006

Received December 1, 2003
Revised February 17, 2004
Accepted February 19, 2004

Gramicidin S has also been the subject of studies of gas-phase ion structure. For example, Williams and co-workers have studied reactions of $[M + 2H]^{2+}$ and $[M + H + X]^{2+}$ ions (where X = Li, Na, or K) with reference bases (i.e., diethylamine) in the gas-phase using ion cyclotron resonance (ICR) mass spectrometry (MS) based techniques [11]. The data presented suggests that the alkali metal binding site of gramicidin S in the gas-phase does not change appreciably with the size of the alkali metal ion. This result is indicative of the relative flexibility of gramicidin S when compared with more sterically hindered, macrocyclcic compounds. Dearden and coworkers have extensively studied the selectivity and binding affinity of crown ether compounds in the gas phase and determined that a preorganized binding site is important for selective alkali binding [12, 13].

Current methods of cyclic peptide identification/analysis rely primarily on mass spectrometry based approaches for final confirmation, although liquid chromatography is often used to monitor the progress of cyclization reactions. For example, Gross and co-workers have developed an iterative ion trap-mass spectrometry method that utilizes multiple stages of mass spectrometry to determine the sequence of a cyclic peptide [14]. However, there are no general methods for determining whether a peptide is cyclic or linear. Ion mobility (IM) separation, which can distinguish small differences in the conformations of gas-phase ions, is a method that can potentially differentiate between cyclic and linear peptides [15, 16]. Recent results from our laboratory suggest that ion mobility can be used to screen peptide mixtures for structural differences. Although there is a high degree of correlation between ion mobility separation and separation based on *m/z* for a homologous series of ions (e.g., singly charged peptides), there is an appreciable degree of scatter (+/−10–15% in drift time) in a plot of drift time versus *m/z* for some ions [17, 18]. This scatter is primarily based on the packing efficiencies of different molecules, different structural classes (i.e., α-helices, β-sheets, etc. in the case of peptides) that develop for a particular ion series, and the influence of metal adduction/covalent modification on gas-phase structure [19, 20].

Here, we describe studies of singly charged, protonated and cationized (Li, Na, K, Rb, Cs), cyclic and linear analogues of gramicidin S ions using matrix assisted laser desorption-ionization (MALDI)-IM-MS to measure the conformation of the gas-phase peptide ions. The aim of these studies is to investigate the role of solvent on the gas-phase structure of gramicidin S, a β-sheet (β-hairpin) standard in solution-phase protein folding studies. In addition, the general ability of IM-MS methods to distinguish cyclic and linear peptides for potential applications in complex mixture screening will be discussed. It is important to note that the cyclic/linear peptide separation efficiency achieved ultimately depends upon the conformational differences observed in the gas-phase between cyclic gramicidin S and its linear analogues. Hypothetically, if no conformational differences are observed, and a cyclic peptide is to be distinguished from linear versions of the same sequence based on gas-phase packing efficiency differences alone, separation would require resolving powers that are beyond the capabilities of current instrumentation, which routinely achieves a resolution of 30-60 [21]. As an additional means of distinguishing cyclic and linear peptide sequences in the gas-phase, collision cross-section (Ω) information as a function of ionizing alkali metal ion is also reported.

Experimental

Sample Preparation

The peptide gramicidin S (denoted **GS** for the remainder of this work) was acquired from Sigma (St. Louis, MO) and linear analogues of gramicidin S were acquired from Enanta Pharmaceuticals Inc. (Watertown, MA) and utilized without further purification. The five linear gramicidin peptide sequences prepared will be referred to as **G1** (VOLFPVOLFP), **G2** (OLFPVOLFPV), **G3**, (LFPVOLFPVO), **G4** (FPVOLFPVOL), and **G5** (PVOLFPVOLF), and represent a break in the cyclic gramicidin S sequence between each amino acid position. Gramicidin related peptides were mixed with bradykinin (*m/z* 1061.2, Ω = 245 Å^2) and substance p (*m/z* 1348.6, Ω = 292 Å^2), both acquired from Sigma, and α-cyano-4-hydroxycinnamic acid (Aldrich, Milwaukee, WI) in a 100:1 matrix to combined analyte ratio for collision cross-section measurement by MALDI-IM-TOF MS using a two-point calibration [22]. For studies involving alkali adduction, a 1–5 μL of a 100 mM chloride salt solution (LiCl, RbCl, or CsCl,) was added in to the MALDI preparation. No added salt was necessary to observe the Na or K adducted peptides. When salt was added, the cationized form was typically the most abundant ion for the gramicidin peptides; however, the cationized peptide ion was rarely the most abundant signal for the internal calibrants (bradykinin and substance p).

Ion Mobility-Mass Spectrometry

The MALDI-IM-TOF MS instrument used in these studies was built in-house and described in detail elsewhere [21]. Briefly, the instrument consists of MALDI ion source equipped with a high repetition rate-frequency tripled (355 nm)-Nd:YAG laser (JDS Uniphase, San Jose, CA) operated at a pulse rate of 200-400 Hz [23], or a cartridge-type Nitrogen laser (337 nm, Thermo Laser Science) operated at a repetition rate of 20 Hz . The drift cell is a 30.5 cm periodic focusing ion mobility drift tube operated at pressures of ~1 torr of He drift gas at room temperature. Under these conditions, the instrument routinely achieves a mobility resolution of 30–60 for peptide ions. After exiting the drift tube the ions are focused by a 5-element einzel lens, through a differen-

tially pumped region (going from 1 torr to ~10^{-3} torr), into an orthogonal extraction source of a 2-stage reflectron time-of-flight mass spectrometer (~1 m path length resolution ~400–1000, operated at 10^{-7} torr). Data is collected on a computer controlled TDC (Ionwerks, Houston TX), using 2-D acquisition software specifically designed for the IM-MS experiment (Ionwerks, Houston, TX). Contour plots shown here are produced using Transform and related programs produced with the IDL software language (Research Systems, Boulder, CO).

Internally Calibrated Measurements of Collision Cross-section

Two-point internal calibration was utilized (with bradykinin and substance p as reference collision cross-sections) to account for the field dependant slope of the drift time-*m/z* relationship [24]. The difference in mobility drift time between both standards and the unknown is measured in multiple runs, and the average collision cross-section (relative to both standards) is reported. All measured collision cross-sections exhibited relative standard deviations of ~1%.

Molecular Dynamics Simulations

Simulated annealing was performed as described previously [19, 20]. Peptide structures were constructed using Insight II (Accelerys, San Diego, CA) and simulated annealing was performed using Cerius^2 version 4.2 (Accelerys). During the first stage of molecular dynamics, several different protonated starting structures were heated over the course of 560 ps in a step-wise fashion, (relaxation time = 0.1 ps, time step = 0.001 ps) starting and ending at 300 K and peaking at 1000 K utilizing the Nosé temperature thermostat (resting at a specific temperature for 10 ps every 50 K). After each annealing cycle, the peptide structure was minimized. Annealing cycles were repeated 100 times for each starting structure, generating 100 minimized structures for any given starting structure, generating a total of ~1200 first stage structures. Structures were then selected on the basis of their fit to experimental collision cross-sections and subjected to further (second stage) calculations, generating ~1000 second stage protonated structures.

Three sites of protonation were investigated for each linear peptide: the N-terminus and the two ornithine side chains, and one of the two equivalent ornithine side chains was chosen for the site of protonation for cyclic gramicidin S. Modeling of the alkali adducts was accomplished by removing the proton from structures generated from second stage simulated annealing and placing a sodium ion in a central position within the peptide for a third stage of molecular dynamics. Simulated annealing was then performed, generating structures from several different linear and cyclic sodiated starting structures, creating a total of ~2000 sodiated peptide structures. Collision cross-sections for all peptide trial structures, including the cross-section based on the crystal structure solved by Dodson and coworkers [8], were calculated using an on-line version of the program developed by Jarrold [25]. In all cases the trajectory method value for the collision cross-section was taken as the calculated value. Visual inspection of the backbone conformation of the peptide was used to classify the structure as part of a group of related structures, and cluster analysis (plots of MD energy versus collision cross-section) was used extensively to identify potential candidates for the final gas-phase structure(s). Although MD energy is not a quantitative measure of the overall stability of a molecule in the gas-phase, it can be used (in a limited fashion) to describe relative differences in stability between gas-phase structures [26].

Circular Dichroism

Spectra were acquired on an Aviv 62DS model CD spectrophotometer (Aviv Associates, Lakewood, NJ). Peptides (**GS**, **G1**, **G2**, **G3**, **G4**, **G5**) were dissolved in 50/50 (vol/vol) H_2O/CH_3OH or 100% 2,2,2 trifluoroethanol (TFE, Aldrich, Milwaukee, WI) at a concentration of 1–2 mg/mL for wavelength scans (0.5 nm/ 3 s, 190–250 nm) both at pH of ~4–5 (measured by pH paper). The spectra were then blank-corrected and subjected to data smoothing (boxcar averaging).

Results and Discussion

Figure 1a contains a plot of drift time versus *m/z* for cyclic and linear gramicidin analogues (**GS** and **G1**). Here, the centroids of the two ion signals differ by 40 μs or 5% of the total average drift time of the two species. Figure 1b shows an equivalent separation for the $[M + H]^+$ and the $[M + Na]^+$ ion of **GS**, separated by 38 μs or ~5% of the total average drift time. The differences in drift time shown in Figure 1a and b are too large to be accounted for by packing efficiency differences for peptide ions with a *m/z* difference of 18 or 22 Da, which are typically indistinguishable by IM separation (i.e., percent difference ~ 0%) [27]. Combined, the observations made in Figure 1a and b illustrate the primary differences observed for these cyclic/linear peptide ions. That is, alkali binding to the cyclic peptide ions increases the collision cross-section by ~5%, whereas the linear peptide ions ($[M + H]^+$ and $[M + Na]^+$) have essentially the same collision cross-section. In addition, the collision cross-section for the linear peptide is similar to the collision cross-sections measured for both the cyclic and linear $[M + Na]^+$.

Figure 2 contains a plot of collision cross-section versus ion type (in order of increasing mass but neglecting the mass difference between GS and linear analogues), which further amplifies on the differences observed for both the cyclic peptide ions (shown in red)

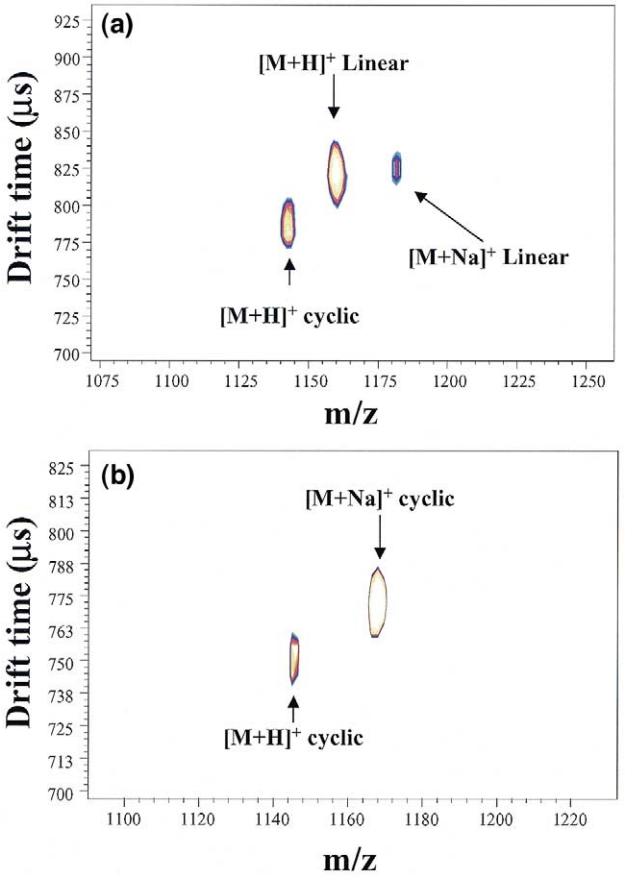

Figure 1. (**a**) Drift time versus *m/z* plot illustrating the mobility separation achieved for cyclic (**GS**) and linear (sequence **G1**) peptides. (**b**) Drift time versus *m/z* plot illustrating the mobility separation achieved for $[M + H]^+$ and $[M + Na]^+$ ions for **GS.** Drift time differences between (**a**) and (**b**) for **GS** are due to run-to-run variations in drift cell pressure.

and the five linear peptide ions (shown in blue). The error bars shown represent 1 σ for the collision cross-section measurements for the $[M + H]^+$, $[M + Li]^+$, $[M + Na]^+$, $[M + K]^+$, $[M + Rb]^+$, and $[M + Cs]^+$ ions of the cyclic and linear peptides. Again, the collision cross-sections for the cyclic and linear peptide $[M + H]^+$ ions are significantly different, the cross-sectional difference decreases substantially between the cyclic and linear $[M + Li]^+$ ions, and all other ion types ($[M + Na]^+$, $[M + K]^+$, $[M + Rb]^+$, and $[M + Cs]^+$) display collision cross-sections that are not significantly different (within 1 σ) between the cyclic and various linear forms of the peptide sequence. It is also important to note that there are no significant differences observed for the collision cross-sections for the linear peptide ions. Hill and co-workers observed different collision cross-sections for different peptide sequences based on a single amino acid substitution, which suggests that amino acid positional isomers (**G1–G5**) might yield a similar effect [28]. Our results suggest that **G5** may have a slightly (~1%) larger collision-cross section than the other linear gramicidin analogues; however, the error of the measurements reported here is not sufficient to claim that the structure of **G5** is different from **G1–G4**. The estimated collision cross-section based on the crystal structure solved by Dodson and coworkers is represented as a dashed line in Figure 2 at 287 Å^2 [8]. The collision cross-sections for the linear protonated and alkylated species are closer to the collision cross-section generated for the crystal structure, the twisted β-sheet structure shown in Figure 3a than the collision cross-section determined for the protonated cyclic peptide (within 1–10 Å^2). However, the cyclic peptide begins to

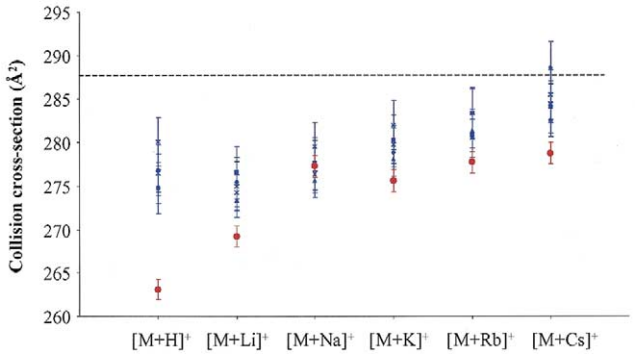

Figure 2. Plot of measured collision cross-section versus ion type (protonated, sodiated, etc.) for all peptides investigated in this work. Data for cyclic **GS** is in red (circles) and data for linear peptides is in blue: **G1** (filled diamond), **G2** (filled square), **G3** (filled triangle), **G4** (x), and **G5** (asterisk). The dashed line represents the calculated collision cross section for the X-ray crystal structure (from reference [8]).

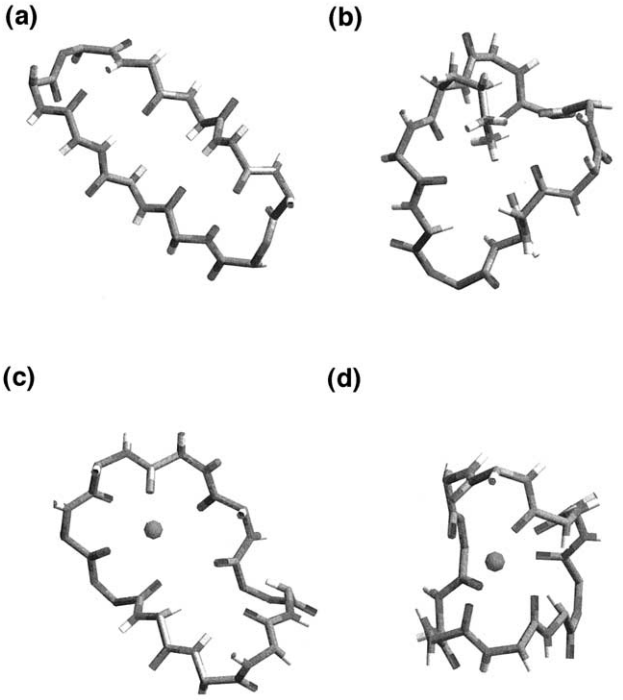

Figure 3. (**a**) The peptide backbone conformation determined by X-ray crystallography for **GS** (taken from reference [8]). (**b**) protonated, (**c**) and (**d**) sodiated conformers produced for the cyclic peptide **GS** from molecular dynamics simulations.

approach the collision cross-section of both the linear peptides and the crystal structure as the size of the alkali ion is increased. Although interesting, it is unclear from the data whether this observation is an effect of the size of the alkali ion or a result of structural transitions in the gas-phase peptides that begin to converge on a configuration that better approximates the crystal structure [8].

To perform an efficient search of the possible conformations of alkali metal-bound peptide ions, we performed molecular dynamics calculations on protonated species and sodiated peptides rather than modeling the influence of a wider range of alkali metals on the structure of the gramicidin cyclic/linear peptides. This approach assumes that the chemistry/binding site of the larger alkali metal ions (Na^+, K^+, Rb^+, and Cs^+) does not vary significantly within the context of peptide binding, and is based on previously reported experimental evidence to that effect. For example, Williams and co-workers have observed similar reaction kinetics for different alkali ion- adducted forms of gas-phase gramicidin s with several gas-phase bases; an observation that suggests that the binding sites of different alkali metals do not vary significantly [11]. A potential exception to this statement may be lithium, because its binding has been characterized as largely non-specific in biological systems [29], a result that is mirrored in some studies of the gas-phase fragmentation of Li^+ cationized peptides [30, 31]. Based on these observations, we chose to focus our modeling data on sodiated peptides, as a model for the influence of Na^+, K^+, Rb^+, and Cs^+ ions, and protonated peptides, as a model for the influence of H^+, realizing that Li^+ cationized peptides may resemble structures from both modeling experiments.

Figure 3 displays three probable (low energy) structures identified from molecular modeling of **GS** in the gas-phase that agree with the measured collision cross-section to within +/−3% (Figure 3b–d), and Figure 3a displays a backbone-only display for the crystal structure determined by Dodson and co-workers [8]. Figure 3b shows the most populated structure (the conformation-type or cluster most often encountered in simulated annealing output) for the protonated cyclic peptide, characterized by a close-packed configuration centered around the charge site (in this case-the ornithine side chain). A high degree of difference is observed when the structure in Figure 3b is compared with the X-ray crystal structure (shown in Figure 3a) for **GS**. Charge site stabilization dominates the protonated structure, as indicated by the large number of carbonyls within 3 Å of the charge site (4 total). Several groups have reported on the influence of charge site on the final gas-phase conformation of proteins and peptides, and manipulation of the charge state/charge position is the primary tool by which gas-phase structural dynamics are studied [32]. When the ionizing proton is replaced with Na^+, molecular dynamics indicates two possible structures: an elongated sheet-type structure where the

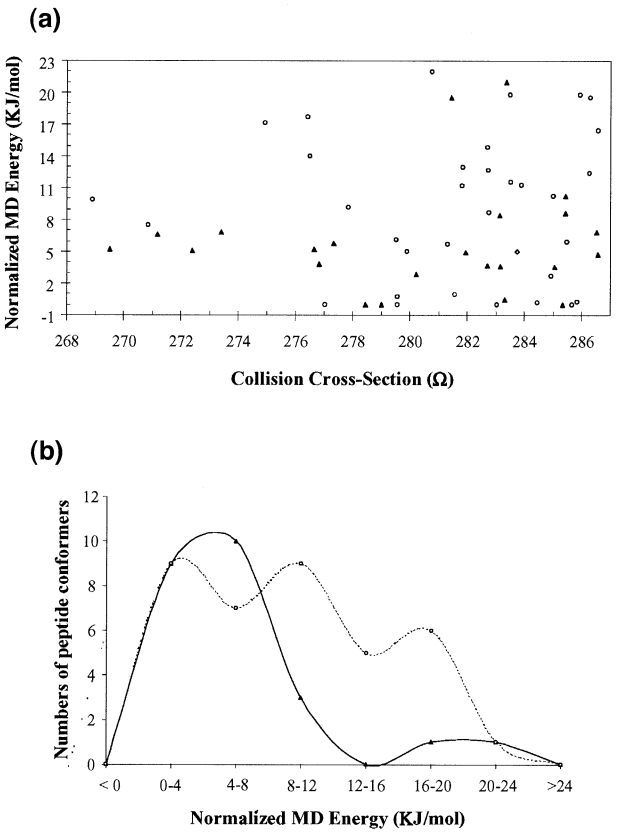

Figure 4. (**a**) Plot of Normalized (to the lowest energy structure(s) in each dynamics run) MD energy versus collision cross-section calculated for conformation from the simulated annealing runs for sodiated **GS**. (**b**) A plot of numbers of peptides versus normalized MD energy for the same data presented in (**a**).

Na^+ is located at one of the turns, or a bent ellipsoid structure were the Na^+ is located near the center of the molecule (Figure 3c and d). The difference in average collision cross-sections for the two structural groups (sheet and ellipsoid) is small, ~1 $Å^2$ on average (280 $Å^2$ and 281 $Å^2$ average collision cross-section respectively), thus it is not possible to distinguish these structures by IM at the resolution of the current instrumentation. Cluster plots of normalized MD energy (where the energy output of the dynamics simulations are all normalized to the lowest energy conformer) versus collision cross-section were used to estimate the relative stability of the two structures (Figure 4a). The points corresponding to the sheet type conformation (Figure 3c: closed, black triangles) are interspersed with those corresponding to the bent-ellipsoid conformation (Figure 3d: open, white circles), which suggests that the two conformations have comparable gas-phase stability. Figure 4b provides a somewhat more detailed picture of the energy distribution for the two identified structural types. This analysis indicates that the centroid of the energy distribution for the sheet-type conformers is shifted to lower energy relative to the more dispersed energy pattern displayed by the bent-ellipsoid conformers. Although cluster analysis seems to favor the sheet-

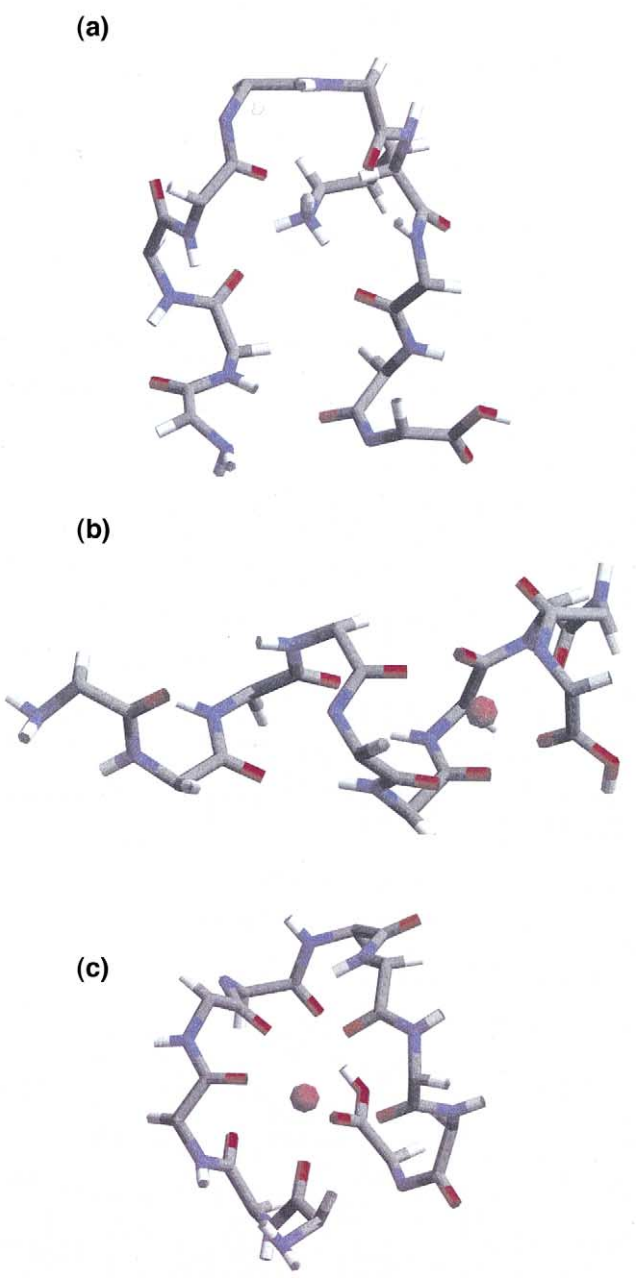

Figure 5. (**a**) Representative protonated structure for linear peptides (**G1**, **G2**, **G3**, **G4**, and **G5**) from MD simulations. (**b**), (**c**) Two potential sodiated peptide structures for the same linear peptides.

type conformation, it is unrealistic to rule out the possibility of a distribution of conformers for the $[M + Na]^+$ **GS** ion that contains both sheet and bent-ellipsoid conformations.

Representative conformations obtained from MD simulations that match the measured collision cross-sections to within +/−3% are shown in Figure 5. For the protonated molecule, MD simulations are dominated by sheet (hairpin) type structures (Figure 5a). It is reasonable to hypothesize that the stability of a sheet-type structure is favored in the linear peptides by increase in H-bonding opportunities over those available in the cyclic structure. Furthermore, it is interesting that we find no evidence that the sequence that comprises the turn (out of the five possible amino acids available in this sequence) within the hairpin structure shown in Figure 5a has little apparent influence on the observed gas-phase structure. Several solution- phase studies have indicated that proline has a rather high-propensity for β-turn formation in both proteins and peptides [33]; however, we find substantial MD evidence for turn formation in all peptides including **G3** where the proline residues are not located in the middle region of the peptide. To date, there has been little gas-phase evidence concerning the formation of sheet-type structures, although there are several studies linking helix formation propensity to amino acid identity [34]. Current evidence from IM studies points to charge-stabilization as the dominant factor in the final conformation of gas-phase peptide ions [16]; a result consistent with the modeling presented here, as the long, flexible ornithine side chain is stabilized through multiple carbonyl interactions present in the turn-region of the peptide.

Figure 5b and c show examples of the two most populated structures from the simulated annealing studies from sodiated linear gramicidin peptide ions. Figure 5b contains a helical conformation stabilized by the favorable interaction of the Na^+ (charge site) with the macro-dipole of the helix. Jarrold and co-workers first observed this type of metal ion induced helix stability in polyalanine systems [35]. The other low-energy conformations identified that match the measured collision cross-sections for the linear peptides, a sheet type structure, is not as energetically favorable as the helix, because the molecule has no stabilizing interaction between the charge site and the macro-dipole. In the cases of the F terminated peptide **G5**, it was observed that the helical conformation was additionally stabilized by a capping interaction between the phenylalanine side chain and the sodium ion. Therefore the MD experiments suggest that there is a high probability that replacing the ionizing proton with a sodium causes a structural transition from a sheet-like to a helical structure in the gas-phase.

The gas-phase conformational assignments for GS and the five linear analogues were compared to solution phase conformation, as determined by circular dichroism (CD), and the spectra are shown in Figure 6. CD data was obtained in two solvent systems, a 50/50 methanol-water solution (to mimic the solvent system utilized for MALDI sample preparation) and 100% TFE. In previous work, we have observed a higher correlation between the TFE solution-phase and the gas-phase peptide ion structures than for either methanol or water-based solvent systems due to the lower dielectric constant and intramolecular H-bond-promoting properties of fluorinated solvent [36]. CD and NMR experiments for **GS** and other cyclic analogues were reported by Hodges and co-workers [10]. On the basis of their data, they proposed three distinct conformational fam-

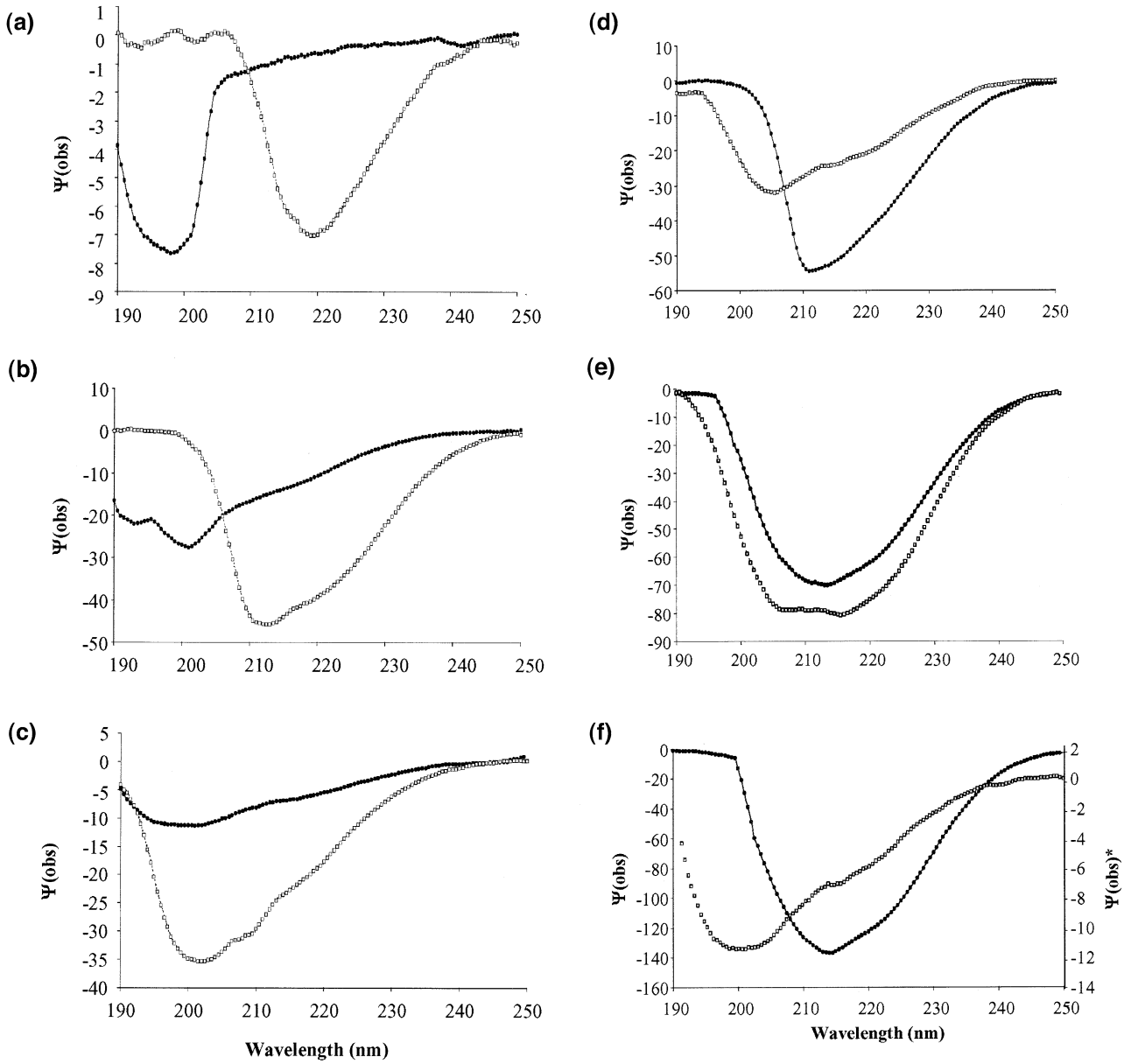

Figure 6. CD spectra for linear and cyclic peptides in two solvent systems: TFE (grey squares) and 50/50 methanol/water (black circles), for the sequences (**a**) **G1**, (**b**) **G2**, (**c**) **G3**, (**d**) **G4**, (**e**) **G5**, and (**f**) **GS**. (Asterisk) The alternate axis for the TFE spectrum of **GS**.

ilies for gramicidin peptides: (1) High (>67%) β-sheet structure, characterized by a broad (in most cases 30 nm), intense minimum at 220 or 225 nm, (2) moderate (30–36%) β-sheet structure, characterized by a broad (25–30 nm) minimum at ~200 nm, and (3) low (<12%) β-sheet content, characterized primarily by a minimum at 200 with decreased spectral features at ~220 nm. The CD results shown in Figure 6 are very similar to those reported by Hodges and co-workers. For example, in 50/50 methanol/water the peptides **G1**, **G2**, and **G3** all exhibit CD spectra similar to those reported for type 3 (low β-sheet content) peptides, but exhibit increased β-sheet content, similar to group 1 for **G1** and **G2** and similar to group 2 for **G3**, in TFE. On the other hand, **G4** and the cyclic **GS** exhibit high β-sheet content in 50/50 methanol-water (similar to group 1) that decreases to moderate β-sheet content in TFE, whereas the β-sheet content of **G5** remains relatively unchanged as a function of solvent. When compared with the gas-phase structures determined by IM, several important differences become apparent: the differences in conformational behavior for the linear gramicidin peptides observed in the CD data are not observed for the gas-phase peptides due to the overriding influence of charge stabilization (rather than amino acid sequence) in the later environment. It is still unclear as to why **G4**

differs from the other linear peptides in terms of reduced of β-sheet content in TFE relative to methanol/water solutions. The overall sequence of **G4** does not contain any potential intramolecular interactions that could disrupt β-sheet formation, especially when compared with the sequences for the other linear gramicidin peptides that show increased β-sheet formation in TFE relative to methanol-water. Such hypotheses can be confirmed by amino acid substitution studies designed to alter the hydrogen-bonding character of the amino acids in the turn. In addition, we plan to investigate the role of solvent on the turn propensities of the amino acids through gas-phase condensation studies [35]. On the other hand, the majority of the conformations indicated by CD data in TFE (5/6) agree well with the gas-phase results for the protonated peptides. In general the comparison of CD data to the gas-phase structures determined by IM and MD simulations indicates that a delicate balance of forces, imparted from both solvent and intramolecular H-bonds, is important for the stabilization of β-sheet type structures.

Conclusions

We have demonstrated that IM is capable of separating cyclic and linear peptides based on structural differences of the gas-phase ions; however, the ability to separate cyclic peptide ions from the linear analogues depends primarily upon the structural preferences of the peptides in question, rather than intrinsic differences in collision cross-section (or packing efficiency differences) between linear and cyclic peptides. Results from Williams and co-workers suggest that the modeling results for Na^+ can be applied (in terms of binding site) to the other larger alkali metals [11]. However, as ionic radius increases, the cyclic peptide may favor the bent ellipsoid structure to the sheet structure based on the strain placed on the turn region of the peptide. Although the CD data suggests that there is an influence of amino acid position on the β-turn propensity of the linear/cyclic peptides, we do not find a similar relationship for cyclic/linear peptide ions in the gas phase. On the other hand, CD measurements performed in TFE agree well with the gas-phase structures measured by IM-MS, which underscores the utility of TFE (and possibly other low dielectric solvents) CD measurements for assigning gas-phase ion structure. A comparison of the conformations measured in each of the environments, gas-phase, TFE, and methanol/water, illustrates the degree to which the β-sheet structure adopted by native gramicidin S (see Figure 3a) is stabilized though interaction with solvent molecules. In addition, comparisons of IM-MS and CD data for linear and cyclic peptide analogues, it appears that either the addition of another hydrogen bonding site (in the case of linear peptide analogues) or the re-positioning of the ionic charge site (as in the alkali adducted cyclic peptides) stabilizes sheet-like structure in the gas-phase. Further experiments, including amino acid substitutions aimed at strengthening the intramolecular hydrogen-bonding character of the peptide and gas-phase solvation experiments [16], will be utilized to clarify the relationship between hydrogen bonding and charge-stabilization on β-sheet (β-hairpin) structure for peptide ions. In the cases of **G1-G3** and **G5**, it is expected that the addition of water molecules to the gas-phase peptide ion will eventually catalyze a transition to a "denatured" β-sheet conformation, whereas, a similar structural transition may not be observed for **G4** or **GS**. Even though IM separation of cyclic/linear peptide is primarily based on structural differences in the gas-phase ions rather than intrinsic differences in the mobility of cyclic and linear peptides, the observed conformational change upon alkali adduction for both linear and cyclic peptides may provide a more general method for distinguishing between linear and cyclic peptides. The general utility of generating alkali adducts of cyclic peptides as a more selective structural tool than collision cross-section measurement alone is currently under investigation in our laboratory.

In addition to the analytical implications of the data presented here, the gas-phase biophysics of **GS** and its linear peptide analogues appear to be a rich system in which to study β-sheet formation in the gas-phase. This investigation is one of the few to report evidence of stable sheet (hairpin) structures in the gas-phase [37, 38], and our future work will focus on the gas-phase structure and dynamics of **GS** and related systems. Cyclic peptides in particular, as molecular systems having a somewhat forced geometry, are particularly interesting as gas-phase standards for peptide structure, as the companion MD simulations that are necessary for the determination of structural detail from collision cross-section measurements are simplified by the restricted degrees of freedom for the peptide system.

Acknowledgments

The authors thank Kent J. Gillig and Shane Tichy (TAMU) for work on supporting experiments, as well as John Benson and Bradly Brasher (Enanta Pharmaceuticals) for providing the linear gramicidin analogues. Funding for this research is provided by the National Science Foundation (CHE-9629966, MRI-0116685), the Texas Advanced Research Program/ Technology Development/ Transfer (TARP/TDT, 010366-0064-2001), the Department of Energy, Division of Chemical Sciences, BES (DE-FG03-95ER14505) and The Robert A. Welch Foundation (A-1176).

References

1. Walters, P. W.; Namchuk, M. A Guide to Drug Discovery: Designing Screens: How to Make Your Hits a Hit. *Nat. Rev. Drug Discov.* **2003,** *2,* 259–266.
2. Oldfield, E. Chemical Shifts in Amino Acids, Peptides, and Proteins: From Quantum Chemistry to Drug Design. *Annu. Rev. Phys. Chem.* **2002,** *53,* 349–378.
3. Muegge, I. Selection Criteria for Drug-Like Compounds. *Med. Res. Rev.* **2003,** *23,* 302–321.

4. Jelokhani-Niaraki, M.; Prenner, E. J.; Kondejewski, L. H.; Kay, C. M.; McElhaney, R. N.; Hodges, R. S. Conformation and Other Biophysical Properties of Cyclic Antimicrobial Peptides in Aqueous Solutions. *J. Peptide Res.* **2001,** *58,* 293–306.
5. Kondejewski, L. H.; Farmer, S. W.; Wishart, D. S.; Kay, C. M.; Hancock, R. E. W.; Hodges, R.S. Modulation of Structure and Antibacterial and Hemolytic Activity by Ring Size in Cyclic Gramicidin S Analogs. *J. Biol. Chem.* **1996,** *271,* 25261–25268.
6. Epand, R. M.; Vogel, H. Diversity of Antimicrobial Peptides and Their Mechanisms of Action. *Biochim. Biophys. Acta* **1999,** *1462,* 11–28.
7. Prenner, E. J.; Lewis, R. N. A. H.; McElhaney, R. N. The Interaction of the Antimicrobial Peptide Gramicidin S with Lipid Bilayer Model and Biological Membranes. *Biochim. Biophys. Acta* **1999,** *1462,* 201–221.
8. Tishchenko, G. N.; Andrianov, V. I.; Vainstein, B. K.; Woolfson, M. M.; Dodson, E. Channels in the Gramicidin S-with-Urea Structure and Their Possible Relation to Transmembrane Ion Transport. *Acta Cryst. D* **1997,** *D53,* 151–159.
9. Lee, D. L.; Hodges, R. S. Structure-Activity Relationships of de Novo Designed Cyclic Antimicrobial Peptides Based on Gramicidin S. *Biopolymers* **2003,** *71,* 28–48.
10. Gibbs, A. C.; Bjorndahl, T. C.; Hodges, R. S.; Wishart, D. S. Probing the Structural Determinants of Type II′ β-Turn Formation in Peptides and Proteins. *J. Am. Chem. Soc.* **2002,** *124,* 1203–1213.
11. Gross, D. S.; Williams, E. R. Structure of Gramicidin S $(M + H + X)^{2+}$ Ions (X = Li, Na, K) Probed by Proton Transfer Reactions. *J. Am. Chem. Soc.* **1996,** *118,* 202–204.
12. Zhang, H.; Dearden, D. V. The Gas-Phase Macrocyclic Effect: Reaction Rates for Crown Ethers and the Corresponding Glymes with Alkali Metal Cations. *J. Am. Chem. Soc.* **1992,** *114,* 2754–2755.
13. Chu, I.; Zhang, H.; Dearden, D. V. Macrocyclic Chemistry in the Gas Phase: Intrinsic Cation Affinities and Complexation Rates for Alkali Metal Cation Complexes of Crown Ethers and Glymes. *J. Am. Chem. Soc.* **1993,** *115,* 5736–5744.
14. Ngoka, L. C. M.; Gross, M. L. Location of Alkali Metal Binding Sites in Endothelin A Selective Receptor Antagonists, Cyclo(D-Trp-D-Asp-Pro-D-Val-Leu) and Cyclo(D-Trp-D-Asp-Pro-D-Ile-Leu), from Multistep Collisionally Activated Decompositions. *J. Mass Spectrom.* **2000,** *35,* 265–276.
15. Hoaglund-Hyzer, C. S.; Counterman, A. E.; Clemmer, D. E. Anhydrous Protein Ions. *Chem. Rev.* **1999,** *99,* 3037–3079.
16. Jarrold, M. F. Peptides and Proteins in the Vapor Phase. *Annu. Rev. Phys. Chem.* **2000,** *51,* 179–207.
17. Ruotolo, B. T.; Gillig, K. J.; Stone, E. G.; Russell, D. H. Peak Capacity of Ion Mobility Mass Spectrometry: Separation of Peptides in Helium Guffer Gas. *J. Chromatogr. B* **2002,** *782,* 385–392.
18. Ruotolo, B. T., Mclean, J. A., Gillig, K. J., Russell, D. H. Peak Capacity of Ion Mobility Mass Spectrometry: The Utility of Varying Drift Gas Polarizability for the Separation of Tryptic Peptides. *J. Mass Spectrom.*, unpublished.
19. Ruotolo, B. T.; Verbeck, G. F.; Thomson, L. M.; Gillig, K. J.; Russell, D. H. Observation of Conserved Solution-Phase Secondary Structure in Gas-Phase Tryptic Peptides. *J. Am. Chem. Soc.* **2002,** *124,* 4214–4215.
20. Ruotolo, B. T.; Verbeck, G. F., IV; Thomson, L. M.; Woods, A. S.; Gillig, K. J.; Russell, D. H. Distinguishing Between Phosphorylated and Nonphosphorylated Peptides with Ion Mobility-Mass Spectrometry. *J. Proteome Res.* **2002,** *1,* 303–306.
21. Gillig, K. J., Ruotolo, B. T., Stone, E. G., Russell, D. H. Periodic Focusing Ion Mobility Spectrometer-Mass Spectrometer, unpublished.
22. Shoff, D. B.; Harden, C. S. Unambiguous Identification fo IMS responses by IMS-MS/MS—Development of Realistic Standards for Ion Mobility Determinations. *Proceedings of the Fourth International Workshop on Ion Mobility Spectrometry*; Cambridge, U.K., 1995.
23. McLean, J. A.; Russell, D. H. Sub-Femtomole Ppeptide Detection in Ion Mobility-Time-of-Flight Mass Spectrometry Measurements. *J. Proteome Res.* **2003,** *2,* 428–431.
24. Ruotolo, B. T.; McLean, J. A.; Gillig, K. J.; Russell, D. H., unpublished.
25. Jarrold, M. F. http://nano.chem.indiana.edu/software.html.
26. Abagyan, R.; Argos, P. Optimal Protocol and Trajectory Visualization for Conformational Searches of Peptides and Proteins. *J. Mol. Biol.* **1992,** *225,* 519.
27. Wyttenbach, T.; von Helden, G.; Bowers, M. T. Gas-Phase Conformation of Biological Molecules: Bradykinin. *J. Am. Chem. Soc.* **1996,** *118,* 8355.
28. Wu, C.; Siems, W. F.; Klasmeier, J.; Hill, H. H. Separation of Isomeric Peptides Using Electrospray Ionization/High-Resolution Ion Mobility Spectrometry. *Anal. Chem.* **2000,** *72,* 391–395.
29. Olsher, U. Coordination Chemistry of Lithium Ion: A Crystal and Molecular Structure Review. *Chem. Rev.* **1991,** *91,* 137–164.
30. Teesch, L. M.; Adams, J. Fragmentations of Gas-Phase Complexes Between Alkali Metal Ions and Peptides: Metal Ion Binding to Carbonyl Oxygens and Other Neutral Functional Groups. *J. Am. Chem. Soc.* **1991,** *113,* 812–820.
31. Grese, R. P.; Gross, M. L. Gas-Phase Interactions of Lithium Ions and Dipeptides. *J. Am. Chem. Soc.* **1990,** *112,* 5098–5104.
32. Hudgins, R. R.; Jarrold, M. F. Helix Formation in Unsolvated Alanine-Based Peptides: Helical Monomers and Helical Dimers. *J. Am. Chem. Soc.* **1999,** *121,* 3494–3501.
33. Voet, D.; Voet, J. G. Biochemistry, 2nd ed; John Wiley and Sons: New York, NY, 1995; p 1361.
34. Chakrabartty, A.; Baldwin, R. L. Stability of α-Helices. *Adv. Protein Chem.* **1995,** *46,* 141–176.
35. Kohtani, M.; Kinnear, B. S.; Jarrold, M. F. Metal-Ion Enhanced Helicity in the Gas Phase. *J. Am. Chem. Soc.* **2000,** *122,* 12377–12378.
36. Ruotolo, B. T.; Russell, D. H., unpublished.
37. Unterberg, C.; Gerlach, A.; Schrader, T.; Gerhards, M. Structure of the Protected Dipeptide Ac-Val-Phe-OMe in the Gas Phase: Towards a β-Sheet Model System. *J. Chem. Phys.* **2003,** *118,* 8296–8300.
38. Li, A.; Fenselau, C.; Kaltashov, I. A. Stability of Secondary Structural Elements in a Solvent-Free Environment. II: The β-Pleated Sheets. *Prot. Struct. Funct. Gen.,* Suppl. 2, **1998,** 22–27.